Study of Rotating Machineries in A Non-Inertial Reference Frame Subjected to Rotations

Cristian Mihail STĂNICĂ
University Politehnica of Bucharest, mihail.stanica@gmail.com

Mihai Valentin PREDOI
University Politehnica of Bucharest, predoi@gmail.com

Ion STROE
University Politehnica of Bucharest, ion.stroe@gmail.com

Abstract: - Rotating machinery operating in non-inertial frames represents a research domain of high interest for the aeronautical, railroad and shipping industries. This paper investigates the variations of rotor frequencies, expressed by the Campbell diagrams, using two models. One model is analytical, providing closed form solutions and considering a rotor with four degrees of freedom. The second model is based on finite elements, Timoshenko beam formulation, for the same rotor.
Campbell diagrams are obtained for both cases using computer codes developed by the first author.
Good agreement between the models at the common eigenmodes, validate the more complex model.

Keywords: - non-inertial, frame, rotordynamics.

1. INTRODUCTION

The inertial reference frame is defined as one in which the second law of Newton is directly applicable [1]. In practice an inertial reference system is dependent of the observer required precision. For example, the building containing a robot could be considered an inertial reference frame for the robot motion, but an Earth's satellite could be described in an inertial reference linked to the Sun.

In many cases it is possible to measure the relative position to a non-inertial reference frame for which the position in time is known, relative to an inertial frame [2]. In accordance with this, any law of motion $f(t)$ where t represents the time, which describes the movement of a non-inertial frame in relation to an inertial one can be developed in a Taylor series [3]:

$$f(t) = q_0 + \dot{q}t + \frac{1}{2!}\ddot{q}t^2 + ... \tag{1}$$

with

$$q_0 = f(0),\ \dot{q} = \frac{df}{dt};\quad \ddot{q} = \frac{d^2 f}{dt^2}. \tag{2}$$

The second law of motion can be deduced using the principle of least action based on the Lagrangean of the mechanical system [4][5]:

$$\delta S = \delta \int L\left(r, \dot{r}, \ddot{r}, ..., \dot{r}^{(n)}\right) dt = 0. \tag{3}$$

From (3) is derived the equation of motion:

$$\frac{\partial L}{\partial r} - \frac{d}{dt}\left(\frac{\partial L}{\partial \dot{r}}\right) + \frac{d^2}{dt^2}\left(\frac{\partial L}{\partial \ddot{r}}\right) - \frac{d^3}{dt^3}\left(\frac{\partial L}{\partial \dddot{r}}\right) + \\ ... + (-1)^n \frac{d^n}{dt^n}\left(\frac{\partial L}{\partial \dot{r}^{(n)}}\right) = 0. \tag{4}$$

This equation translates in the fact that any body will follow a trajectory for which the difference between the kinetic energy and the potential energy is minimum.[6]

In this paper are deduced the differential equations of motion for an elastic rotor in a non-inertial frame following the approach in ref. [7]. A practical application using a rotor model provided in ref. [8] is conducted. New integration cases are presented.

2. PROBLEM FORMULATION

2.1. The reference frames and their relations in terms of translational and angular speed

In order to deduce the dynamic equilibrium equation, three reference frames are used. One inertial $O_0X_0Y_0Z_0$, one non-inertial linked to the casing of the rotating machine $O_1X_1Y_1Z_1$ and one linked to the rotor, more precisely to the disk of the rotor $O_2X_2Y_2Z_2$, with the origin in its mass center. These reference frames are presented in the next figures, and

the absolute rotational speeds involved with each reference system are presented acting along their axes. Their precise role is depicted in the figure 1 where one can observe the axis O_1Z_1 along the centers of the rotating machine bearings and the axis O_2Z_2 tangent to the shaft axis in the disk center of mass.

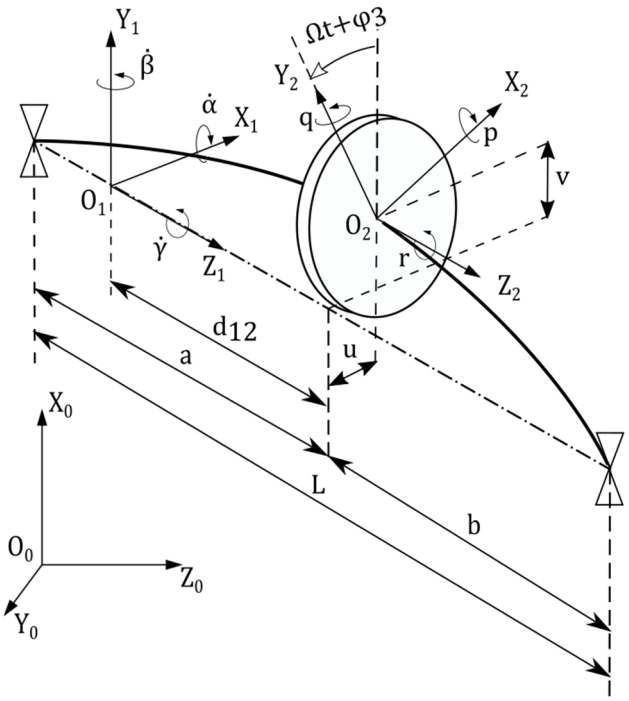

Figure 1. Rotor with notations and reference systems.

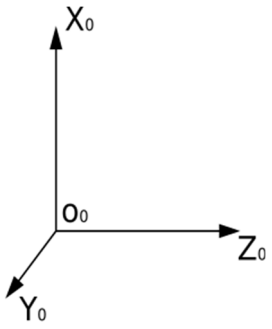

Figure 2a. Inertial reference system.

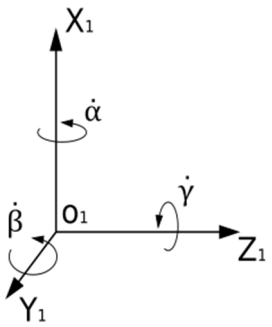

Figure 2b. Non-inertial reference system.

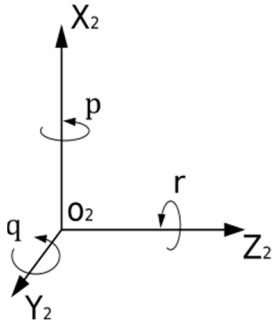

Figure 2c. Disk linked reference system.

In order to deduce the rotational speeds p, q, r of the $O_2X_2Y_2Z_2$ reference frame, one needs to assess the Euler transformation from $O_1X_1Y_1Z_1$ using the XYZ type transformation with the angles φ_1, φ_2, $\Phi_3 = \Omega t + \varphi_3$.[9]

The corresponding transformation matrices are

$$[T_{1-2a}] = \begin{bmatrix} 1 & 0 & 0 \\ 0 & \cos\varphi_1 & -\sin\varphi_1 \\ 0 & \sin\varphi_1 & \cos\varphi_1 \end{bmatrix}, \tag{5}$$

$$[T_{2a-2b}] = \begin{bmatrix} \cos\varphi_2 & 0 & \sin\varphi_2 \\ 0 & 1 & 0 \\ -\sin\varphi_2 & 0 & \cos\varphi_2 \end{bmatrix}, \tag{6}$$

$$[T_{2b-2}] = \begin{bmatrix} \cos\Phi_3 & -\sin\Phi_3 & 0 \\ \sin\Phi_3 & \cos\Phi_3 & 0 \\ 0 & 0 & 1 \end{bmatrix}. \tag{7}$$

In order to obtain the transformation matrix from $O_1X_1Y_1Z_1$ to $O_2X_2Y_2Z_2$, the intermediary transformation matrices are multiplied.

$$[T_{1-2}] = [T_{1-2a}] \cdot [T_{2a-2b}] \cdot [T_{2b-2}]. \tag{8}$$

$$[T_{2-1}] = [T_{1-2}]^T = [T_{2b-2}]^T \cdot [T_{2a-2b}]^T \cdot [T_{1-2a}]^T = \\ = [T_{2-2b}] \cdot [T_{2b-2a}] \cdot [T_{2a-1}]. \tag{9}$$

Using the following notations

$$\begin{aligned} &s_1 = \sin\varphi_1,\ s_2 = \sin\varphi_2,\ s_3 = \sin\Phi_3, \\ &c_1 = \cos\varphi_1,\ c_2 = \cos\varphi_2,\ c_3 = \cos\Phi_3, \end{aligned} \tag{10}$$

the $[T_{1-2}]$ matrix can be expressed as

$$[T_{1-2}]=\begin{bmatrix} c_2c_3 & -c_2s_3 & s_2 \\ c_1s_3+s_1s_2c_3 & c_1c_3-s_1s_2s_3 & -s_1c_2 \\ s_1s_3-c_1s_2c_3 & c_1s_2s_3+s_1c_3 & c_1c_2 \end{bmatrix}. \quad (11)$$

In the next figure are detailed the three successive transformations using two intermediary axis systems $O_{2a}X_{2a}Y_{2a}Z_{2a}$ and $O_{2b}X_{2b}Y_{2b}Z_{2b}$.

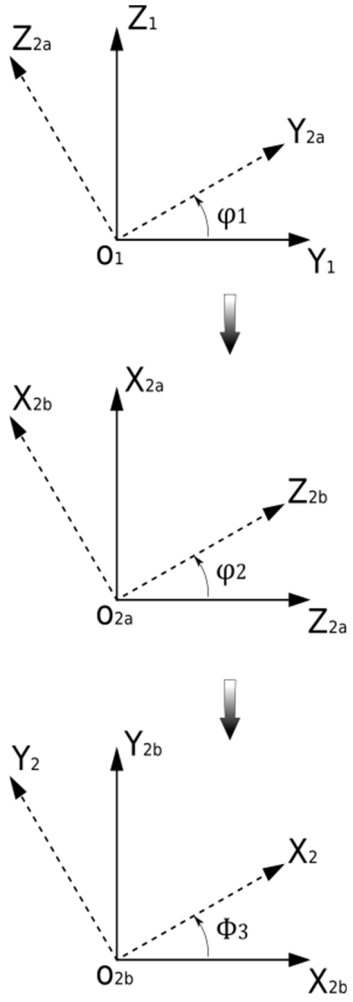

Figure 3. Type XYZ Euler transformation from $O_1X_1Y_1Z_1$ to $O_2X_2Y_2Z_2$.

Regarding the rotational speed, in order to assess the contribution of the Euler angles time variation, the following equality is used [10]

$$\{\omega_{2Euler}\}=[T_{2-2b}]\cdot[T_{2b-2a}]\begin{Bmatrix}\dot\varphi_1\\0\\0\end{Bmatrix}+[T_{2-2b}]\begin{Bmatrix}0\\\dot\varphi_2\\0\end{Bmatrix}+$$
$$+\begin{Bmatrix}0\\0\\\dot\Phi_3\end{Bmatrix}=\begin{bmatrix}c_2c_3 & s_3 & 0\\ -c_2s_3 & c_3 & 0\\ s_2 & 0 & 1\end{bmatrix}\cdot\begin{Bmatrix}\dot\varphi_1\\\dot\varphi_2\\\dot\Phi_3\end{Bmatrix} \quad (12)$$

The rotational speed of the $O_2X_2Y_2Z_2$ reference frame will summarize the Euler angles variation and the rotational speed of the first reference frame. Therefore

$$\{\omega_{20}\}=\begin{Bmatrix}p\\q\\r\end{Bmatrix}=\{\omega_{2Euler}\}+\{\omega_{12}\}=$$
$$=\begin{bmatrix}c_2c_3 & s_3 & 0\\ -c_2s_3 & c_3 & 0\\ s_2 & 0 & 1\end{bmatrix}\cdot\begin{Bmatrix}\dot\varphi_1\\\dot\varphi_2\\\dot\Phi_3\end{Bmatrix}+T_{2-1}\begin{Bmatrix}\dot\alpha\\\dot\beta\\\dot\gamma\end{Bmatrix}. \quad (13)$$

$$\begin{Bmatrix}p\\q\\r\end{Bmatrix}=\begin{Bmatrix}s_3(\dot\varphi_2+\dot\gamma s_1+\dot\beta c_1)+\\ s_3(s_2(c_1\dot\gamma-s_1\dot\beta)-\\ s_2(\dot\varphi_1+\dot\alpha)+\\ +c_3(s_2(\dot\beta s_1-\dot\gamma c_1)+c_2(\dot\varphi_1+\dot\alpha))\\ -c_2(\dot\varphi_1+\dot\alpha))+c_3(\dot\gamma s_1+\dot\beta c_1+\dot\varphi_2)\\ +c_2(\dot\gamma c_1-\dot\beta s_1)+\dot\Phi_3\end{Bmatrix}. \quad (14)$$

For the translational speeds of the disk mass center the fact that the reference frame $O_2X_2Y_2Z_2$ is chosen with the origin in the disk mass center results that the speeds of this will be zero in this reference frame. Therefore, the speed of the origin O_2 in the $O_0X_0Y_0Z_0$ will be the speed of the disk. The speed of origin O_2 will be calculated by adding the speed of the shaft displacements with the speed of transport of the $O_1X_1Y_1Z_1$ reference frame.[2] Index 'd' is denoting the disk.

$$\overline{v}_{20}=\overline{v}_{d0}=\overline{v}_{21}+\overline{v}_{10}+\overline{\omega}_{10}\times\overline{O_1O_2}, \quad (15)$$

Considering that $\overline{v}_{10}$ is null vector by choice, the distance between O_1 origin and O_2 origin is noted d_{12}, and u, v, w are the displacements in $O_1X_1Y_1Z_1$ reference frame. Then for the disk center of mass,

$$\begin{Bmatrix}v_{xd0}\\v_{yd0}\\v_{zd0}\end{Bmatrix}=\begin{Bmatrix}\dot u_d\\\dot v_d\\\dot w_d\end{Bmatrix}+\underbrace{\begin{Bmatrix}0\\0\\0\end{Bmatrix}+\begin{bmatrix}0 & -\dot\gamma & \dot\beta\\ \dot\gamma & 0 & -\dot\alpha\\ -\dot\beta & \dot\alpha & 0\end{bmatrix}\begin{Bmatrix}u_d\\v_d\\d_{12}+w_d\end{Bmatrix}}_{\text{speed of transport}}, \quad (16)$$

$$\begin{Bmatrix} v_{xd0} \\ v_{yd0} \\ v_{zd0} \end{Bmatrix} = \begin{Bmatrix} \dot{u}_d + \dot{\beta}\left(d_{12} + w_d\right) - \dot{\gamma} v_d \\ \dot{v}_d + \dot{\gamma} u_d - \dot{\alpha}\left(d_{12} + w_d\right) \\ \dot{w}_d + \dot{\alpha} v_d - \dot{\beta} u_d \end{Bmatrix} \quad (17)$$

In the above equation w_d and $\dot{w}_d$ can be neglected being very small comparing with u_d, v_d and their corresponding speeds.

2.2. Formulation of the dynamic equilibrium equations using Lagrange formalism

The present approach is limited to the first order acceleration type of non-inertial problems therefore the Lagrange equation has the form [4]

$$\frac{d}{dt}\left(\frac{\partial L}{\partial \dot{q}_k}\right) - \frac{\partial L}{\partial q_k} = 0. \ \text{(k=1, 2, 3, 4)} \quad (18)$$

The Lagrange kinetic potential (eq. 29) includes the kinetic energy *E* and the potential energy *V*. The notation q_k represents the generalized coordinates. The general coordinates are in this case two displacements in translation and two displacements in the rotational angle of the disk mass center.

The kinetic energy can be separated into the translational kinetic energy E_t and the rotational kinetic energy E_r.

$$E = E_t + E_r, \quad (19)$$

Using the simplified approach one can consider the shaft as massless and the disk as rigid and therefore the full kinetic energy is concentrated in the disk. As a consequence, the translational energy of the disk is

$$E = \frac{m_d}{2}\left(v_{xd0}^2 + v_{yd0}^2 + v_{zd0}^2\right) + \\ + \frac{1}{2}\left[I_d\left(p^2 + q^2\right) + I_p r^2\right], \quad (20)$$

where $v_{id0}(i = x, y, z)$ are the translational speeds of the disk and p, q, r are the absolute rotational speeds of the disk calculated along $O_2X_2Y_2Z_2$ axes regarding the inertial reference system $O_0X_0Y_0Z_0$, I_d is the mass-moment of inertia along the disk diameter, I_p is the mass-moment of inertia along the rotational axis of the disk and m_d is the disk mass.

Regarding the potential energy, this is defined in the shaft only, considering that the rotor is rigid. The translation and rotation of the rotor are the considered degrees of freedom. The equations governing the deformation of a simply supported beam are available in the classical stress analysis theory and for this paper the following will be used [8],[11]:

$$F_x = 3EI \cdot \left(\frac{a^3 + b^3}{a^3 \cdot b^3} \cdot u + L\frac{(a-b)}{a^2 \cdot b^2} \cdot \varphi_2\right), \quad (21)$$

$$M_y = 3EI \cdot \left(L\frac{(a-b)}{a^2 \cdot b^2} \cdot u + \frac{L}{a \cdot b} \cdot \varphi_2\right), \quad (22)$$

Using the same pattern, the F_y and M_x are defined. Finally using the notations [11]

$$k_{11} = 3EI \cdot \frac{a^3 + b^3}{a^3 \cdot b^3}, \quad (23)$$

$$k_{14} = 3EI \cdot L\frac{(a-b)}{a^2 \cdot b^2}, \quad (24)$$

$$k_{44} = 3EI \cdot \frac{L}{a \cdot b} \cdot \quad (25)$$

and the above equations can be organized in the matrix form [11]

$$\begin{Bmatrix} F_x \\ F_y \\ M_x \\ M_y \end{Bmatrix} = \begin{bmatrix} k_{11} & 0 & 0 & k_{14} \\ 0 & k_{11} & -k_{14} & 0 \\ 0 & -k_{14} & k_{44} & 0 \\ k_{14} & 0 & 0 & k_{44} \end{bmatrix} \cdot \begin{Bmatrix} u \\ v \\ \varphi_1 \\ \varphi_2 \end{Bmatrix}, \quad (26)$$

Usually the potential energy V in a linear elastic system can be expressed using matrix notation

$$V = \frac{1}{2}\{F\}^T \cdot \{q\} = \frac{1}{2}\{q\}^T [K] \cdot \{q\} \cdot \quad (27)$$

Generally, when a rotor is subjected to inertial forces these will generate a component along the axis of the rotor bearings. Therefore, depending where is placed the axial bearing of the rotor shaft relating to the direction of the inertial force, the shaft can be subjected to tension or compression. This tension status is influencing the overall stiffness of the shaft contributing to the lateral displacement modification. In order to account for this phenomenon, an additional stiffness matrix can be employed which

will couple the displacement along Z1 axis (w) with the displacement along X1 (u) and Y1 (v) axes. This was studied and implemented by Kosmatka [12] in the Timoshenko beam theory and remains a future development of formulation presented in this paper. Notation k_L and k_{tor} are used for the axial stiffness of the rotor shaft and torsional stiffness.

$$V = \frac{k_{tor}\varphi_3^{\,2}}{2} + \frac{k_{44}\left(\varphi_2^{\,2} + \varphi_1^{\,2}\right)}{2} + k_{14}\left(u\varphi_2 - v\varphi_1\right) + \\ + \frac{k_L w^2}{2} + \frac{k_{11}\left(v^2 + u^2\right)}{2}. \tag{28}$$

Using the equations (14), (17), (20) and (28) one can obtain the Lagrangean function for this application.

$$L = E - V. \tag{29}$$

Further using equations (18) the dynamic equilibrium equations are obtained. In order to obtain a solvable linear equation system, the small terms are approximated by linear terms and the second order small terms are eliminated such as the Lagrange equations (18) becomes

$$\ddot{u}\cdot m_d - 2\cdot m_d\cdot\dot{\gamma}\cdot\dot{v} + \\ + u\cdot\left(-\dot{\gamma}^2 m_d - \dot{\beta}^2 m_d + k_{11}\right) + \\ + v\cdot\left(\dot{\alpha}\cdot\dot{\beta}\cdot m_d\right) + \varphi_2\cdot k_{14} + m_d\cdot d_{12}\cdot\dot{\alpha}\cdot\dot{\gamma} = 0 \tag{30}$$

$$\ddot{v}\cdot m_d + 2\cdot m_d\cdot\dot{\gamma}\cdot\dot{u} + \\ + v\cdot\left(-\dot{\gamma}^2 md - \dot{\alpha}^2 md + k_{11}\right) + \\ + u\cdot\left(\dot{\alpha}\cdot\dot{\beta}\cdot m_d\right) - \varphi_1\cdot k_{14} + m_d\cdot d_{12}\cdot\dot{\beta}\cdot\dot{\gamma} = 0 \tag{31}$$

$$\ddot{\varphi}_1\cdot I_d + \dot{\varphi}_2.\left(I_p\Omega + I_p\dot{\gamma} - 2I_d\dot{\gamma}\right) + \\ + \varphi_1\cdot\left(I_p\dot{\gamma}\cdot\Omega + k_{44} + I_p\dot{\gamma}^2 - I_d\dot{\gamma}^2 - I_p\dot{\beta}^2 + I_d\dot{\beta}^2\right) + \\ + \varphi_2\cdot\left(I_p\dot{\alpha}\dot{\beta} - I_d\dot{\alpha}\dot{\beta}\right) - k_{14}\cdot v + I_p\cdot\dot{\beta}\left(\Omega + \dot{\gamma}\right) = 0 \tag{32}$$

$$\ddot{\varphi}_2\cdot I_d + \dot{\varphi}_1\cdot\left(-I_p\Omega - I_p\dot{\varphi}_3 - I_p\dot{\gamma} + 2I_d\dot{\gamma}\right) + \\ + \varphi_2\left(I_p\dot{\gamma}\cdot\Omega + k_{44} + I_p\dot{\gamma}^2 - I_d\dot{\gamma}^2 - I_p\dot{\alpha}^2 + I_d\dot{\alpha}^2\right) + \\ + \varphi_1\left(I_p\dot{\alpha}\dot{\beta} - I_d\dot{\alpha}\dot{\beta}\right) + k_{14}u - I_p\dot{\alpha}\cdot\left(\Omega + \dot{\gamma}\right) = 0 \tag{33}$$

Arranging the terms of Lagrange equation in matrix form results the following equation,

$$[M]\{\ddot{q}\} + \left(\Omega\cdot[G] + \dot{\gamma}\cdot[C_d]\right)\{\dot{q}\} + \\ + \left([K] + \dot{\alpha}^2[K_{d1}] + \dot{\beta}^2[K_{d2}] + \dot{\gamma}^2[K_{d3}] + \right. \\ \left. + \dot{\alpha}\dot{\beta}[K_{d4}] + \dot{\gamma}\cdot\Omega[K_{d5}]\right)\{q\} + \{F\} = 0. \tag{34}$$

The coefficients matrices are defined as

$$[M] = \begin{bmatrix} m_d & 0 & 0 & 0 \\ 0 & m_d & 0 & 0 \\ 0 & 0 & I_d & 0 \\ 0 & 0 & 0 & I_d \end{bmatrix} \tag{35}$$

$$[G] = \begin{bmatrix} 0 & 0 & 0 & 0 \\ 0 & 0 & 0 & 0 \\ 0 & 0 & 0 & I_p \\ 0 & 0 & -I_p & 0 \end{bmatrix} \tag{36}$$

$$[C_d] = \begin{bmatrix} 0 & -2m_d & 0 & 0 \\ 2m_d & 0 & 0 & 0 \\ 0 & 0 & 0 & I_p - 2I_d \\ 0 & 0 & -I_p + 2I_d & 0 \end{bmatrix} \tag{37}$$

$$[K_{d1}] = \begin{bmatrix} 0 & 0 & 0 & 0 \\ 0 & -m_d & 0 & 0 \\ 0 & 0 & 0 & 0 \\ 0 & 0 & 0 & -I_p + I_d \end{bmatrix} \tag{38}$$

$$[K_{d2}] = \begin{bmatrix} -m_d & 0 & 0 & 0 \\ 0 & 0 & 0 & 0 \\ 0 & 0 & -I_p + I_d & 0 \\ 0 & 0 & 0 & 0 \end{bmatrix} \tag{39}$$

$$[K_{d3}] = \begin{bmatrix} -m_d & 0 & 0 & 0 \\ 0 & -m_d & 0 & 0 \\ 0 & 0 & I_p - I_d & 0 \\ 0 & 0 & 0 & I_p - I_d \end{bmatrix} \tag{40}$$

$$[K_{d4}]=\begin{bmatrix} 0 & m_d & 0 & 0 \\ m_d & 0 & 0 & 0 \\ 0 & 0 & 0 & I_p-I_d \\ 0 & 0 & I_p-I_d & 0 \end{bmatrix} \quad (41)$$

$$[K_{d5}]=\begin{bmatrix} 0 & 0 & 0 & 0 \\ 0 & 0 & 0 & 0 \\ 0 & 0 & I_p & 0 \\ 0 & 0 & 0 & I_p \end{bmatrix} \quad (42)$$

[K] is defined in (26). The terms in the above matrices are confirmed by [13] albeit the axis orientation, the type of Euler transformation and the order of the freedom degrees is different in this paper and therefore the position of the terms in the matrices is different regarding [13].

The above equation contains a set of constant terms presented as forces and moments. These are grouped in the column matrix $\{F\}$ .These constant forces determines an equilibrium position around which the vibration is developing. In order to solve for natural frequencies, the homogenous system is used which lacks the $\{F\}$ generalized forces column matrix.[14]

In equation (34) considering the terms $\dot{\alpha}$, $\dot{\beta}$ and $\dot{\gamma}$ constants, after adding and multiplying it becomes by notation

$$[M]\{\ddot{q}\}+[C_T]\{\dot{q}\}+[K_T]\{q\}=\{0\}. \quad (43)$$

2.3. Application in the finite element domain

The matrices deduced for the non-inertial dynamic equilibrium of the rotor can be extended in the finite element model in order to account for the influence of the shaft to the overall behavior of the whole rotor. One way to do this is to consider a very small slice of the rotor shaft with the thickness ds and to treat it as a small rotor disk. Then its mass will be

$$m_d=\rho\cdot\pi\cdot R^2\cdot ds=\rho\cdot A\cdot ds. \quad (44)$$

And its rotational mass-moments of inertia will be

$$I_d=\rho\cdot I\cdot ds,\quad I=\pi R^4/4, \quad (45)$$

$$I_p=2\cdot I_d. \quad (46)$$

The shaft can be split in zones of length L_e which will be considered as finite elements. The small disk considered of thickness ds is positioned at the s position inside a finite element. Its corresponding non-inertial matrices are defined in (37) - (42).

The notation $\{d_s\}$ is used for the small disk four displacements (two translations, two rotations).

$$\{d_s\}=\{u_s \quad v_s \quad \varphi_{1s} \quad \varphi_{2s}\}^T. \quad (47)$$

One fundamental property of the finite element in general is that a displacement inside the element can be expressed as a function of the element extremities displacements $\{q_e\}$. These functions are known as shape functions. If it is used the notation of Ψ for the (translations and rotations) shape functions matrix, [11] such as

$$\{d_s\}=[\Psi(s)]\cdot\{q_e\}, \quad (48)$$

$$\{q_e\}=\{u_1 \; v_1 \; \theta_{x1} \; \theta_{y1} \; u_2 \; v_2 \; \theta_{x2} \; \theta_{x2}\}^T, \quad (49)$$

Then the terms of kinetic energy for the finite element can be written in matrix form. As an example, using (47)-(49),

$$\frac{1}{2}\int_0^{L_e} m_d\dot{u}_s^2 =$$

$$=\frac{1}{2}\rho A\{\dot{q}_e\}^T\int_0^{L_e}\left([\Psi(s)]^T\begin{bmatrix} 1&0&0&0 \\ 0&0&0&0 \\ 0&0&0&0 \\ 0&0&0&0 \end{bmatrix}[\Psi(s)]\right)ds\{\dot{q}_e\} \quad (50)$$

The Lagrangean terms are then arranged in matrix form like (50) and the Lagrange equations are formulated in matrix form.

$$\frac{d}{dt}\left(\frac{\partial T}{\partial\{\dot{q}_e\}}\right)-\frac{\partial V}{\partial\{q_e\}}=\{0\}. \quad (51)$$

The integrals like those provided in relation (50) are not affected by the derivations in the Lagrange equations (51) and are passed unchanged in the results. The potential energy for Timoshenko formulation is presented in [11]. Finally, the dynamic equilibrium equation in the matrix form is obtained identical with the simplified case (34) albeit the matrices are defined for Timoshenko beam. The non-inertial stiffness matrices for the finite element have the form

$$\left[K_{di}^{e}\right]=\int_{0}^{L_e}\left(\left[\Psi(s)\right]^{T}\cdot\left[K_{di}\right]\cdot\left[\Psi(s)\right]\right),\ i=1...5. \tag{52}$$

$\left[K_{di}\right]$ from (38)-(42). Finally, $\left[C_{d}^{e}\right]$ matrix in finite element formulation, results in the form

$$\left[C_{d}^{e}\right]=\int_{0}^{L_e}\left(\left[\Psi(s)\right]^{T}\cdot\left[C_{d}\right]\cdot\left[\Psi(s)\right]\right). \tag{53}$$

The integrals are split in two, one for the translational terms and the other for rotational terms. For example, for the $\left[K_{d1}^{e}\right]$ matrix considering the relations (38) (44-46) and a shaft element with constant section characteristics I, A.

$$\left[K_{d1}^{e}\right]=$$
$$=-\rho A\int_{0}^{L_e}\left(\left[\Psi(s)\right]^{T}\cdot\begin{bmatrix}0&0&0&0\\0&1&0&0\\0&0&0&0\\0&0&0&0\end{bmatrix}\cdot\left[\Psi(s)\right]\right)ds-$$
$$-\rho I\int_{0}^{L_e}\left(\left[\Psi(s)\right]^{T}\cdot\begin{bmatrix}0&0&0&0\\0&0&0&0\\0&0&0&0\\0&0&0&1\end{bmatrix}\cdot\left[\Psi(s)\right]\right)ds. \tag{54}$$

The same procedure is applied to all the non-inertial matrices and finally the integrals will result in a set of matrices dependent of the shape functions multiplied by the characteristic terms of beam like area, density and area moment of inertia in order to obtain the non-inertial finite element matrices. The matrices $[M],[G],[K]$ for Timoshenko beam are the usual, inertial ones defined in [8][11].

3. THE SOLUTION FOR THE DYNAMIC EQUATIONS OF EQUILIBRIUM

Using the notations and further matrix arrangement

$$\{X\}=\begin{Bmatrix}\dot{q}\\q\end{Bmatrix}, \tag{55a}$$

$$[A]=\begin{bmatrix}[M]&0\\0&[I]\end{bmatrix}, \tag{55b}$$

$$[B]=\begin{bmatrix}[C_T]&[K_T]\\[-I]&0\end{bmatrix}, \tag{55c}$$

the equation (43) becomes [11]:

$$[A]\{\dot{X}\}+[B]\{X\}=\{0\}. \tag{56}$$

This can be reduced further to a classical eigenvalues formulation problem by choosing

$$\{X\}=\{Y\}\cdot e^{\lambda\cdot t},\ \{\dot{X}\}=\lambda\cdot\{Y\}\cdot e^{\lambda\cdot t} \tag{57}$$

and multiplying (56) with $-[A]^{-1}$ such as

$$-\lambda\cdot\{Y\}\cdot e^{\lambda\cdot t}-[A]^{-1}[B]\{Y\}\cdot e^{\lambda\cdot t}=\{0\}. \tag{58}$$

Simplifying for the term $\cdot e^{\lambda\cdot t}$ the (58) becomes

$$-[A]^{-1}[B]\{Y\}=\lambda\cdot\{Y\}. \tag{59}$$

The imaginary part of λ eigenvalue represents the system damped natural frequencies. The lower half of $\{Y\}$ eigenvectors can be noted with $\{y\}$. These occurs in pairs of complex numbers and their conjugate. Their assembling provides the solution of the initial problem.

$$\{q\}(t)=\{y\}\cdot e^{\lambda t}+\{y\}^{*}\cdot e^{\lambda^{*}t}. \tag{60}$$

Usually in the design process, the resonances with excitation forces like rotor imbalance are forbidden. Therefore, a safety margin is applied to the operation domain of the rotating machine in relation with the natural frequencies. For this purpose, the Campbell diagram tool is used.

4. PRACTICAL APPLICATION OF THE DEVELOPED THEORY

In order to verify the presented theory, a practical example is presented. A rotor with a shaft L=1.1m long and diameter d_s=0.038m is supported by rigid bearings at the extremities. Also, a disk is fitted on the shaft at a distance noted with 'a' from one extremity of the shaft and noted with 'b' regarding the opposite extremity of the shaft. (See figure 1.) The radius of the disk is R_d=0.325m and the thickness is h_d=0.1m. The material is steel with density $7810\cdot kg/m^3$, Young modulus $E=2.11\cdot10^{11}\cdot N/m^2$. For this case we choose

the distance between the reference systems $|O_1O_2|=d_{12}=0$ and a=b=L/2. Considering this data, the area moment of inertia of the shaft is [8][11]

$$I=\frac{\pi}{64}\cdot d_s^4=1.023538741\cdot 10^{-7}\ \left[m^4\right]. \quad (61)$$

For the disk the mass and mass-moment of inertia are

$$m_d=\rho\cdot\pi\cdot {R_d}^2\cdot h_d=259.16\ \left[\mathrm{kg}\right], \quad (62)$$

$$I_d=\frac{m_d}{12}\cdot\left(3\cdot R_d^2+L_d^2\right)=7.0594\ \left[kg\cdot m^2\right], \quad (63)$$

$$I_p=\frac{m_d}{2}\cdot R_d^2=13.687\ \left[\mathrm{kg\cdot m^2}\right]. \quad (64)$$

Using these, the stiffness matrix terms can be computed

$$k_{11}=3EI\cdot\frac{a^3+b^3}{a^3\cdot b^3}=\ 778843\ \left[\mathrm{N/m}\right], \quad (65)$$

$$k_{14}=3EI\cdot L\frac{(a-b)}{a^2\cdot b^2}=0\ \left[\mathrm{N}\right], \quad (66)$$

$$k_{44}=3EI\cdot\frac{L}{a\cdot b}=\ 235600\ \left[\mathrm{N\cdot m}\right]. \quad (67)$$

The formulas are confirmed by the data from ref. [8][11].

4.1. Jeffcott rotor in the inertial frame

In the **inertial case** ($\dot{\alpha}=0,\ \dot{\beta}=0,\ \dot{\gamma}=0$) considering that $k_{14}=0$ one can observe that the first two equation lines in (34) can be decupled and solved individually such as the first two natural frequencies are obtained

$$\omega_{1,2}=\sqrt{\frac{k_{11}}{m_d}}=54.82\left[rad/s\right]=8.7\left[Hz\right]. \quad (68)$$

Further, the other two lines of equations concerning the angular displacements degrees of freedom, we have the following natural frequencies [8][11]:

$$\omega_3=-\frac{I_p\cdot\Omega}{2I_d}+\sqrt{\left(\frac{I_p\cdot\Omega}{2I_d}\right)^2+\frac{k_{44}}{I_d}}, \quad (69a)$$

$$\omega_4=+\frac{I_p\cdot\Omega}{2I_d}+\sqrt{\left(\frac{I_p\cdot\Omega}{2I_d}\right)^2+\frac{k_{44}}{I_d}}. \quad (69b)$$

One can observe that $\omega_{1,2}$ does not depend of the rotational speed Ω and are constant. In case of ω_3 and ω_4 for $\Omega=0$

$$\omega_{3,4}=\sqrt{\frac{k_{44}}{I_d}}=182.68\left[rad/s\right]=29.1\left[Hz\right], \quad (70)$$

and for $\Omega=3000\ rpm=314.16\ rad/s$, $\omega_3=8.05\ Hz$, $\omega_4=105\ Hz$. Finally we can conclude that the Campbell diagram for the usual inertial case, when $\dot{\alpha}=0,\ \dot{\beta}=0,\ \dot{\gamma}=0$, consists of four vibration lines, two constant at 8.7Hz and two variable with the rotational speed starting both at 29.1Hz and ending at 8.05Hz and 105Hz for the maximum rotational speed.

One very important aspect in rotating machines operation is the calculation of critical rotational speeds. These rotational speeds should be avoided with a 5-10% margin during operation and should be passed fast during startup or shutdown of the machine. These dangerous rotational speeds correspond to the intersections of the natural frequencies with the excitation lines in the Campbell diagram. For example, the (F1/N1) crossing take place when $\Omega_{cr}=F_1$. F_1 in the Campbell diagram correspond with ω_1 in the domain 0-2750 rpm and with ω_3 in the domain 2750-3000 rpm. Therefore

$$\begin{aligned}&\Omega_{cr}(F1/N1)=8.7\left[Hz\right]=8.7\left[rps\right]=522\left[rpm\right],\\&\Omega_{cr}(F2/N1)=\Omega_{cr}(F1/N1)=17\%N_n.\end{aligned} \quad (71)$$

For determining $\Omega_{cr}(F3/N1)$ one can observe in figure 4 that it corresponds to ω_3 determined analytically in equation (69a). Therefore, by making $\omega_3=\Omega$ the $\Omega_{cr}(F3/N1)$ can be found as

$$\begin{aligned}\Omega_{cr}(F3/N1)&=\sqrt{\frac{k_{44}}{I_d+I_p}}=\\&=106.56\left[rad/s\right]=\\&=1017.6\left[rpm\right]=34\%N_n\end{aligned} \quad (72)$$

Considering a safety margin of 10% results a continuous working range of $37-100\%N_n$.

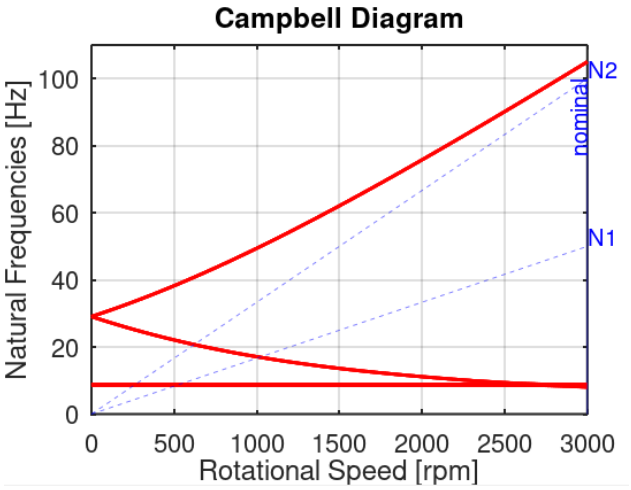

Figure 4. Campbell diagram for the usual case when $O_1X_1Y_1Z_1$ is an inertial frame.

4.2. Jeffcott rotor in a non-inertial reference frame with angular speeds.

First case we choose ($\dot{\alpha}=8rps,\ \dot{\beta}=0,\ \dot{\gamma}=0$)

The solution to the dynamic equilibrium equations of the Jeffcott rotor is easy observing that the majority of the non-inertial matrices are multiply by zero and just K_{d1} remain to be multiplied by $\dot{\alpha}^2$.

The equations still can be decupled in this case such as for the X direction the resulting natural frequency remains as defined in (68). For the Y direction, according to (34), the non-inertial term must be added to the k_{11} stiffness resulting the natural frequency corresponding Y direction

$$\omega_2=\sqrt{\frac{k_{11}-\dot{\alpha}^2 m_d}{m_d}}=21.88\left[rad/s\right]=3.48\left[Hz\right]. \tag{73}$$

The same reason is applying to the rotation vibration on Y axis. The rotation stiffness k_{44} is modified by addition of the non-inertial term provided by the $\left[K_{d1}\right]$ matrix resulting the bending stiffness $k_{44}+\dot{\alpha}^2(-I_p+I_d)$. Therefore, for $\Omega=0$ the two natural frequencies ω_3 and ω_4 will be no more identical but the difference will be

$$\Delta\omega=\frac{\sqrt{\frac{k_{44}}{I_d}}-\sqrt{\frac{k_{44}-\dot{\alpha}^2(I_p-I_d)}{I_d}}}{2\pi}=1.05\left[Hz\right]. \tag{74}$$

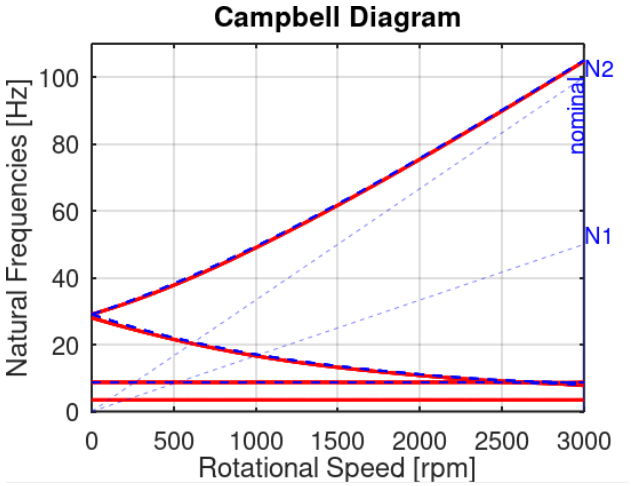

Figure 5. Campbell diagram: $\dot{\alpha}=8rps, \dot{\beta}=0, \dot{\gamma}=0$
(Blue interrupted line = inertial case for reference)

In this case the crossings are

$$\begin{aligned}&\Omega_{cr}(F1/N1)=209\left[rpm\right]=7\%N_n,\\&\Omega_{cr}(F2/N1)=523\left[rpm\right]=17\%N_n,\\&\Omega_{cr}(F3/N1)=999\left[rpm\right]=33\%N_n.\end{aligned} \tag{75}$$

This results in a continuous working range for the rotating machine of $36-100\%N_n$ with 10% safety margin regarding $(F3/N1)$ crossing.

The second case we consider the same rotational speed $\omega_{10}=8rps$ but distributed between X1 and Z1 axes such as

$$\left(\dot{\alpha}=8rps\cdot\sin\frac{\pi}{4},\ \dot{\beta}=0,\ \dot{\gamma}=8rps\cdot\cos\frac{\pi}{4}\right).$$

In this case the equations are no more decupled and using the eigenvectors calculation method the Campbell diagram in figure 6 is obtained.

In this case one can observe an important modification of the crossing's values in comparison with the inertial case and the previous non-inertial case.

$$\begin{aligned}&\Omega_{cr}(F1/N1)=103\left[rpm\right]=3\%N_n,\\&\Omega_{cr}(F2/N1)=808\left[rpm\right]=27\%N_n,\\&\Omega_{cr}(F3/N1)=1153\left[rpm\right]=38\%N_n.\end{aligned} \tag{76}$$

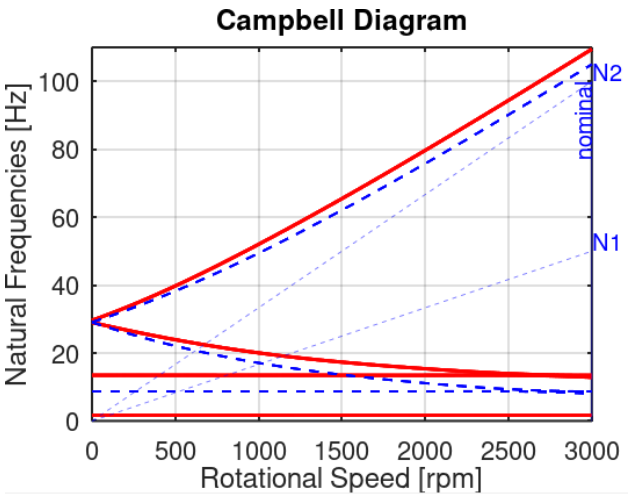

Figure 6. Campbell diagram $\dot{\alpha} \neq 0, \dot{\beta} = 0, \dot{\gamma} \neq 0$. (Blue interrupted line = inertial case for reference)

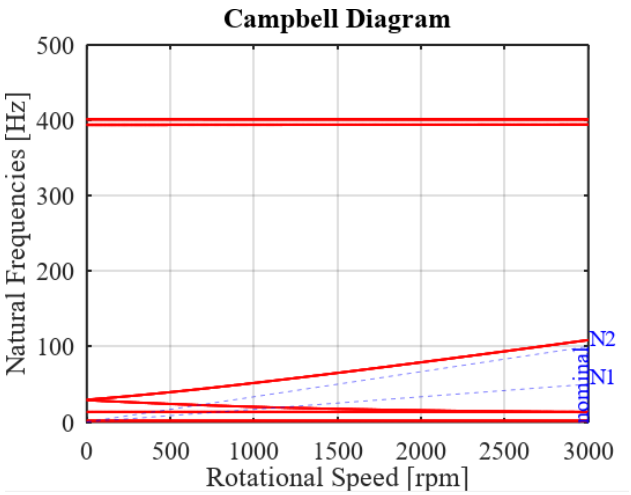

Figure 7. Campbell diagram $\dot{\alpha} \neq 0, \dot{\beta} = 0, \dot{\gamma} \neq 0$. Timoshenko finite element formulation.

Using a 10% safety margin the continuous working range for the rotating machine will be $42 - 100\% N_n$.

Using the simplified model with just four degrees of freedom is a satisfactory approach for simple geometries when the mass of the rotor greatly exceeds the mass of the shaft. Just four natural frequencies can be obtained by this method. If it is necessary to investigate the superior natural frequencies or to clearly evaluate the vibration shapes and the precession of the shaft then it is mandatory to use the finite element method. Also, the finite element method is mandatory if the mass of the rotor disk is comparable with the mass of the rotor shaft or it is smaller.

As an example, for this problem the vibration shapes evaluated at the nominal rotational speed (N_n) of 3000rpm are provided in the following figures. In the next figures the numbering convention for vibration lines is decided by the order the natural frequencies appear at each rotational speed similar with [15] and not by the number of associate vibration shape determined analytically.

The first vibration shape which is depicted in figure 8 is a translation vibration developed mainly along the Y axis with elliptical orbits. Its decreased value comparing with inertial case is due to the spin softening generated by the $\dot{\alpha}$ rotational speed.

The second vibration shape is a disk rotation vibration accompanied by the shaft bending and a precession moment which produce a backward precession and reduces the natural frequency proportional with the rotational speed Ω.

The third vibration shape (figure 10) is a translational vibration mainly along X axis.

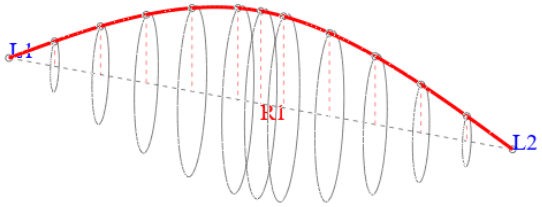

Figure 8. Vibration shape and precession orbits for F1=1.6Hz at 3000rpm for Campbell in fig.7.

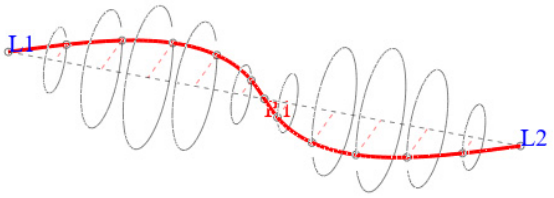

Figure 9. Vibration shape and precession orbits for F2=12.8Hz at 3000rpm for Campbell in fig.7.

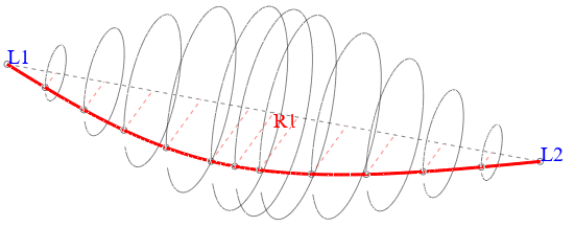

Figure 10. Vibration shape and precession orbits for F3=13.3Hz at 3000rpm for Campbell in fig.7.

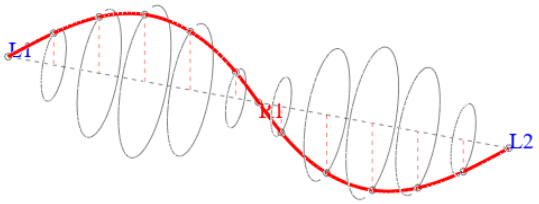

Figure 11. Vibration shape and precession orbits for F4=108.6Hz at 3000rpm for Campbell in fig.7.

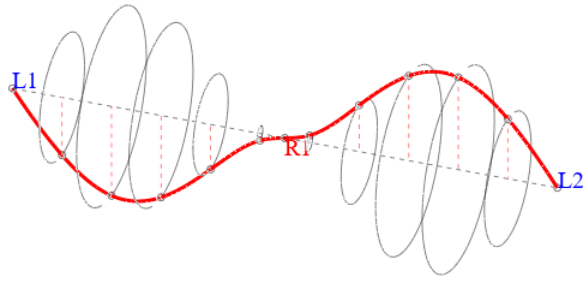

Figure 12. Vibration shape and precession orbits for F5=394.2Hz at 3000rpm for Campbell in fig.7.

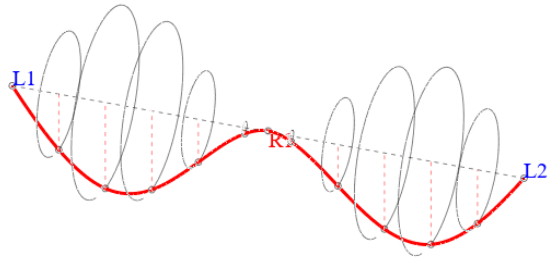

Figure 13. Vibration shape and precession orbits for F6=394.2Hz at 3000rpm for Campbell in fig.7.

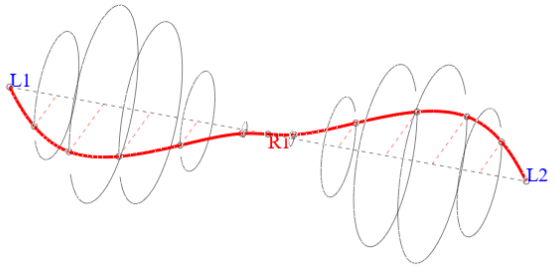

Figure 14. Vibration shape and precession orbits for F7=400.9Hz at 3000rpm for Campbell in fig.7.

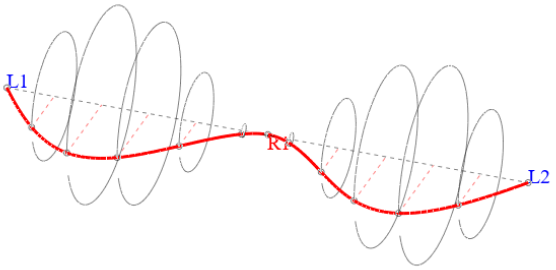

Figure 15. Vibration shape and precession orbits for F8=401.8Hz at 3000rpm for Campbell in fig.7.

The F4 vibration shape is a rotation disk vibration paired with F2 which is accompanied by a gyroscopic moment which rises the associate natural frequency. Finally, the F5 – F8 vibration shapes are shaft vibration shapes in which the rotor is practically still and just the shaft is vibrating. Due to the presence of $\dot{\alpha}$ rotational speed the vibrations along Y axis have smaller natural frequencies than the same shapes vibrating mainly along X direction because the spin softening effect.

Another effect which affects all vibration shapes is the gyroscopic moment generated by $\dot{\gamma}$ rotational speed and which amplify the difference between the pair vibration shapes like F1-F3, F5-F7 and F6-F8. This is done by the matrices $[C_d]$, $[K_{d3}]$ and $[K_{d5}]$. One can observe that the $\dot{\alpha}$ rotational speed generated a spin softening which acts only in the plan perpendicular to the vector $\bar{\dot{\alpha}}$ due to the matrix K_{d1}. In contrast $\dot{\gamma}$ rotational speed generate a spin softening that affects the translational vibration along both lateral directions due to the matrix K_{d3}.

Analyzing the Campbell diagram for crossings one can observe that the dangerous zones associated with the vibration lines crossing the excitation lines is considerably modified once the non-inertial rotational speed is applied.

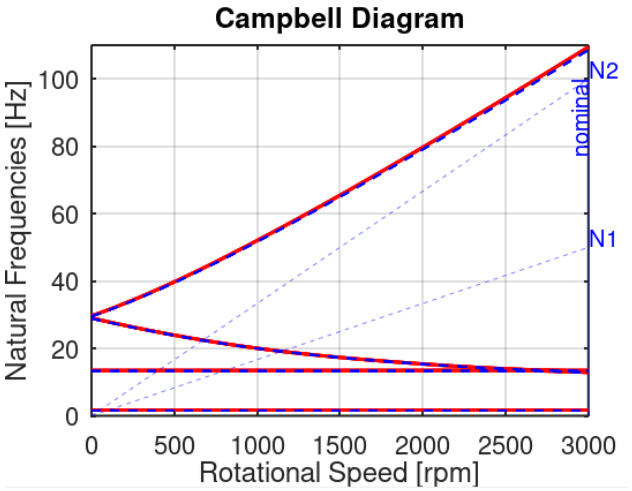

Figure 16. Campbell diagram $\dot{\alpha} \neq 0, \dot{\beta} = 0, \dot{\gamma} \neq 0$. Comparison between analytical solution and Timoshenko finite element formulation. (red continuous line=analytical, blue interrupted line=Timoshenko)

Regarding the difference between the finite element method and the analytical method from the figure 16 we can conclude for simple cases like Jeffcott rotor the Campbell diagram is practically identical. Small difference began to develop towards the high natural frequencies.

One interesting application of the results can be for example, an electrical pump in the temperature management system of an unmanned space capsule which is designed to spin with the rotational speed $\bar{\omega}_{10}$. The case presented in the figure 17 can be reduced to the above analysis adjusting accordingly the rotor characteristics and considering

$$\dot{\alpha} = |\omega_{10}| \sin \nu, \quad \dot{\gamma} = |\omega_{10}| \cos \nu. \qquad (77)$$

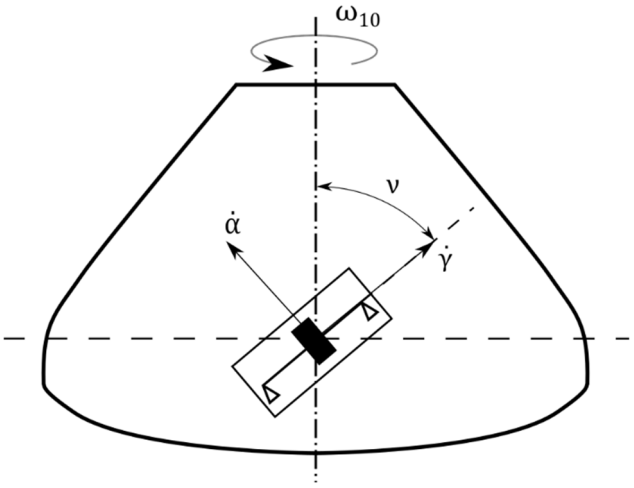

Figure 17. Rotating machine in a rotating space capsule.

5. CONCLUSIONS

When the rotating machineries are involved in activities with strong non-inertial character their analysis, design and assembly should be assessed using the presented theory. In this paper, a practical example was considered and the case of a non-inertial rotating reference frame, linked to the rotating machinery. In relation with the figure 17, the vibrations of the machine were studied for two values of the angle between the rotational speed of the non-inertial reference frame and the machine bearings axis $(\nu = \pi / 2, \text{ and } \nu = \pi / 4)$. It was demonstrated that the working range in terms of rotational speed is considerably affected due to the changing of the crossings in the Campbell diagram. The continuous working regime was reduced with 5% of nominal rotational speed (N_n) comparing with the inertial operation range. Also, depending of the application, the F1 could be constrained to other type of safety margin regarding 0Hz value at which the rotor will fail. (F1=1.3Hz can be unacceptably close to 0Hz for many applications) Additionally, the crossings with the other excitation lines N2, N3 etc. can be checked using the same methodology like for N1. A good agreement regarding the matrices and formulas was found with others authors in the field like [8] and [12].

Also, the finite element method developed perfectly agrees with the analytical calculations and greatly enhances the capability of analyzing high complexity parts and higher frequencies domains.

The final conclusion is that the non-inertial study is critical and is absolutely necessary to be done for space craft applications, as well as for all activities which involves high speeds in a non-inertial reference frames.

ACKNOWLEDGMENTS

The first author would like to thank Ministry of National Education for granting his research for a Ph.D. thesis at the University Politehnica of Bucharest and the guidance of the Ph.D. committee at the Faculty of Biotechnical Systems Engineering.

REFERENCES

[1] Isaac Newton., *Mathematical Principles of Natural Philosophy*, 1687.
[2] Stroe I., Craifaleanu A. Generalization of the Lagrange Equations Formalism, for Motions with Respect to Non-Inertial Reference Frames, *Applied Mechanics and Materials*, Vol. 656 (2014) pp 171-180, Trans Tech Publications, Switzerland
[3] Kamalov T.F., *Physics of Non-Inertial Reference Frames*, Moscow State Open University.
[4] Lagrange J.I., *Mécanique analytique*, Paris, De Saint, 1788.
[5] Ostrogradsky M., *Mem. De l'Acad. De St.-Petersburg*, v. 6, p. 385, 1850.
[6] Feynman R.P., *Principles of Least Action in Quantum Mechanics*, Princeton University, 1942.
[7] Voinea R., Stroe I., Vibrations of Rotors Situated in Non-Inertial Reference Frame, *Mécanique-Matériaux-Electricité, Revue du GAMI*, numéro 446, pp. 58-60, 1992.
[8] Friswell M. I., Penny J. E. T., Garvey S. D., and Lees A. W., *Dynamics of Rotating Machines,* Cambridge, New York, Cambridge University Press, 2010.
[9] *Robot Dynamics Lecture Notes*, Robotic Systems Lab, ETH Zurich HS, https://ethz.ch , 2017.
[10] Leng G., Flight Dynamics, Stability & Control, http://dynlab.mpe.nus.edu.sg .
[11] Chen J.W., Gunter J.E., Introduction *to Dynamics of Rotor Bearing Systems*, Victoria, B.C., Trafford, 2005.
[12] Kosmatka J.B., An improved two-node finite element for stability and natural frequencies of axial-loaded Timoshenko beams, *Computers and Structures*, Vol.57, no.1, pp 141-149, 1995.
[13] Han Q., Chu F., Parametric Instability of flexible rotor-bearing system under time-periodic base angular motions, *Applied Mathematical Modelling,* Vol.39, p4511-4522,2015
[14] Stanica M.C., Stroe I., Vibration of rotor blades with large deformations in a rotating noninertial reference frame, *U.P.B. Scientific Bulletin, Series D*, Vol.80, Iss.2, 2018.
[15] Gu X.J. and all, Free vibration of rotating cantilever pre-twisted panel with initial exponential function type geometric imperfection, *Applied Mathematical Modelling*, Vol.68, Pages 327-352, ISSN 0307-904X, 2019.